

Sounding Rocket Fin Design to Mitigate Roll Lock-In

C.P.Hoult (*Author*)
Rocket Science and Technology
4363 Motor Ave.
Culver City, CA 90232
(310) 839-8959
houltight@aol.com

Hien Tran (*Author*)
Rocket Science and Technology
2822 W. Borchard Ave
Santa Ana, CA 92704
hienttran@gmail.com

Abstract— Roll lock-in is a persistent high angle of attack, nonlinear coning motion sometimes observed in the flight of reentry vehicles and sounding rockets. For example, it has occurred during Aerobee sounding rocket and Sidewinder missile flights prior to the introduction of rollerons. This paper focuses on how fin design effects the probability of lock-in. The high angle of attack response is driven by misalignment and/or offset thrust and drag forces, amplified by during pitch-roll resonance. High angles of attack engender nonlinear roll moments which cause the roll rate to follow the pitch natural frequency. It is well known that such roll moments can arise when the center of mass is offset from the vehicle symmetry axis. However, this paper explores another source of nonlinear high angle of attack roll moments, interaction between vorticity shed from a fore body and tail fins. Both kinds of roll moment have similar magnitudes. However, lock-in due to center of mass offset is, apart from static margin, not affected by fin design.

The location and strength of the shed vortex pair are found from wind tunnel data. Roll moments are estimated from strip theory assuming incompressible cross flow. Conditions for steady state roll lock-in, and its probability of occurrence, are derived from the rigid body moment equations. A technique for significantly reducing the probability of roll lock-in by adjusting the fin exposed semispan and static margin is presented, and used to show that, for a typical university sounding rocket, static margins larger than the classical two caliber heuristic rule can mitigate this problem. Fin taper ratio was studied, and found to have a relatively minor effect. Little difference between three and four fins was found. But, more than four fins, at fixed static margin, can significantly reduce the incidence of roll lock-in. Six fins are much better than four, and eight are better still.

TABLE OF CONTENTS

I.	INTRODUCTION	1
II.	NOTATION	2
III.	VORTEX PAIR DESCRIPTION	3
IV.	ANALYSIS OF VORTEX-INDUCED ROLL MOMENT.....	4
V.	LOCKED-IN LUNAR MOTION	5
VI.	EXAMPLE.....	7
VII.	IMPLICATIONS FOR FIN DESIGN	8
VIII.	RECOMMENDATION.....	10
	REFERENCES	10
	APPENDIX I: STABILITY DERIVATIVES	10
	APPENDIX II: CENTER OF MASS OFFSET MOMENT.....	12

I. INTRODUCTION

Roll lock-in, or catastrophic yaw, is the most challenging, non-linear phenomenon in the field of sounding rocket dynamics. There are several causes for this phenomenon: First, poor design leads to configurational asymmetries. Second, lateral offset of the center of mass relative to the symmetry axis leads to both pitch/yaw perturbing torques, and to nonlinear roll moments. Finally, the interaction of fore body vortices and tail fins causes nonlinear, high angle of attack roll moments. Since only the last is significantly relevant to fin design, it is the only one studied here. Note, however, that the first two have generally valid remedial design prescriptions, e. g., roll balancing.

Experience has shown that sounding rocket roll lock-in usually begins in powered flight at the time of yaw-roll resonance when a rocket's pitch/yaw natural frequency equals its roll rate¹. During resonance the angle of attack response to body-fixed perturbations is significantly amplified. Re-entry vehicles are similarly afflicted during yaw-roll resonance². Then nonlinear roll moments will compel the roll rate to follow the yaw natural frequency indefinitely. Such locked-in motion is said to be lunar with one side of the rocket always facing the cone axis. The consequence is a prolonged period of excessive drag with severe adverse effects on the mission. The body-fixed perturbations driving all this are random. Therefore, for a given rocket flying a given mission, the occurrence of roll lock-in is also random.

In the past, most studies of roll lock-in have focused on nonlinear transient phenomena^{1,4}. But, some previous studies^{3,4} have shown that catastrophic yaw is a continuing (quasi-steady state) process. Two significant aerodynamic nonlinearities, Magnus moment and vortex-induced roll moment, are important. Our approach is to first estimate the steady state coning rate from the yaw moment equation, and, using the pitch moment equation, the fin panel size to ensure the desired (input) vehicle static margin is attained. Next, the minimum angle of attack for which steady state lunar roll lock-in is possible is found from the roll moment equation. The probability of no roll lock-in is the objective function for optimizing fin design, and is estimated from known body-fixed perturbations^{15,16}.

II. NOTATION

Mnemonic	Definition		
a	Distance from a vortex core to a point on a fin,	g	Indefinite integral in the roll moment induced by a single fin by a single vortex,
b	Exposed semispan of a fin,	I_P	Pitch/yaw moment of inertia,
C_D	Fin airfoil drag coefficient for a section normal to the leading edge,	L	Rocket overall length,
$C_{D\alpha\alpha}$	$= \frac{\partial^2 C_D}{\partial \alpha^2}$,	l_T	Distance from the nozzle to the rocket center of mass,
$C_{M\alpha}$	Pitching moment coefficient slope,	M	Free stream Mach number,
C_N	Normal force coefficient of the entire vehicle,	N	Number of fin panels,
$C_{N\alpha}$	Fin span-average airfoil normal force coefficient slope without any body interference,	Pr	Probability on no roll lock-in,
$C_{N\alpha F}$	Fin assembly normal force coefficient slope,	p, q, r	Roll, pitch and yaw rates,
$C_{N\alpha N}$	Nose normal force coefficient slope,	q	Dynamic pressure,
C_L	Roll moment coefficient $C_L \equiv L/qSd$,	R	Body radius,
$C_{L\delta}$	Single fin roll moment coefficient due to fin cant,	r	Distance from the body centerline to the core of a free vortex,
C_{Li}	Amplitude of the vortex-induced roll moment coefficient,	S	Aerodynamic reference area = πR^2
C_{Lp}	Roll moment coefficient due to fin damping in roll,	SM	Pitch/yaw static margin,
C_{LV}	Nonlinear roll moment due to interaction between nose vorticity and tail fins,	s	Distance from the body centerline to the core of an image vortex,
C_{LO}	Nonlinear roll moment coefficient due to CG offset,	T	Thrust force,
C_{Np}	Yawing moment coefficient due to roll rate,	U	Free stream velocity,
$C_{Np\alpha}$	Yawing moment coefficient due to roll rate and angle of attack,	v_θ	Tangential velocity around a vortex,
C_{Nr}	Yawing moment coefficient due to yaw rate,	v_N	Velocity normal to a fin panel,
C_Y	Magnus side force coefficient per unit length based on cross flow velocity,	x	Distance aft of the nose tip,
$c(y)$	Local fin chord at spanwise station y ,	x_{CG}	Distance from the nose tip to the Center of Gravity,
c_R	Root chord,	x_{CPF}	Distance from the nose tip to the fin assembly center of pressure,
c_T	Tip chord,	x_{CPN}	Distance from the nose tip to the nose center of pressure,
d	Aerodynamic reference length = $2R$,	x_S	Distance aft of the nose tip where vortex separation occurs,
f_i	Integral functions,	y	Distance from the body centerline to a point on a fin,
		y_V	Lateral distance from the body centerline to a free vortex core,
		z_V	Vertical distance from the body centerline to a free vortex core,
		α	Body angle of attack,
		α^*	Minimum angle of attack for which lock-in can occur,

α_{local}	Local angle of attack at a point on a fin,
β	Dimensionless exposed semispan $= b/R$,
δ	Fin cant angle,
δ_T	Single plane thrust misalignment angle,
ϕ	Body roll angle,
ϕ_V	Roll angle attitude of a free vortex,
Γ	Circulation around a free vortex,
Λ	Fin sweep back angle, between root chord and leading edge,
λ	Fin taper ratio $= c_T/c_R$,
ω	Coning rate,
ω_n	Pitch/yaw natural frequency, and
Ω	Single plane center of mass offset,
$(\)_o$	Value of $(\)$ at low angle of attack.

III. VORTEX PAIR DESCRIPTION

It will probably come as no surprise to the reader to find that there is an extensive literature on the vortex wakes in the lee of slender bodies of revolution^{5,6,7}. These will provide what we need to know.

Our chosen point of departure is the longitudinal location x_s where the vortex pair separates from the body. While this is difficult to accurately determine experimentally, it would appear that the separation point approximately corresponds to the location where the zero α static pressure on the body is a minimum. Aft of this point, the longitudinal pressure gradient is adverse, i.e., pressure increasing as x increases. This is a strong argument for locating the vortex separation point there. In Fig. 1 the definitions are:

$$\text{Dimensionless Distance Aft of Separation} = \frac{(x - x_s)\alpha}{R}$$

$$\text{Dimensionless Vortex Strength} = \frac{\Gamma}{2\pi R U \alpha}$$

Using these definitions, the empirical data in Fig. 1 can be well represented by

$$\frac{\Gamma}{2\pi R U \alpha} = 0.6 + 0.08 \left[\frac{(x - x_s)\alpha}{R} \right]^{1.52} \quad (1)$$

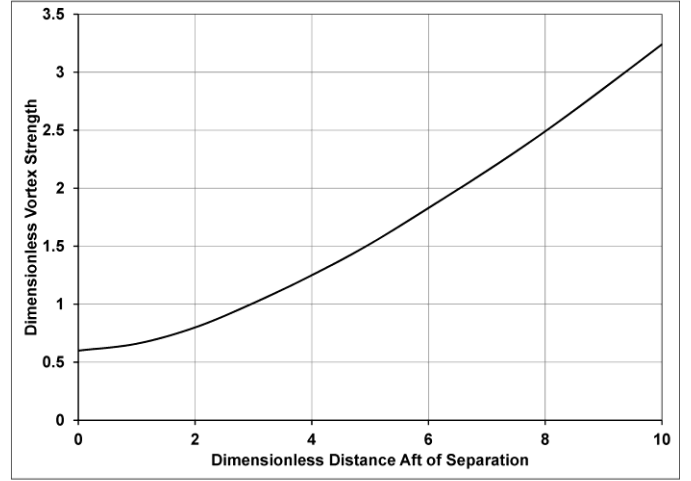


Figure 1 - Free Vortex Strength

The approximate lateral location y_V of a vortex core is

$$\frac{y_V}{R} = 0.7 \quad (2)$$

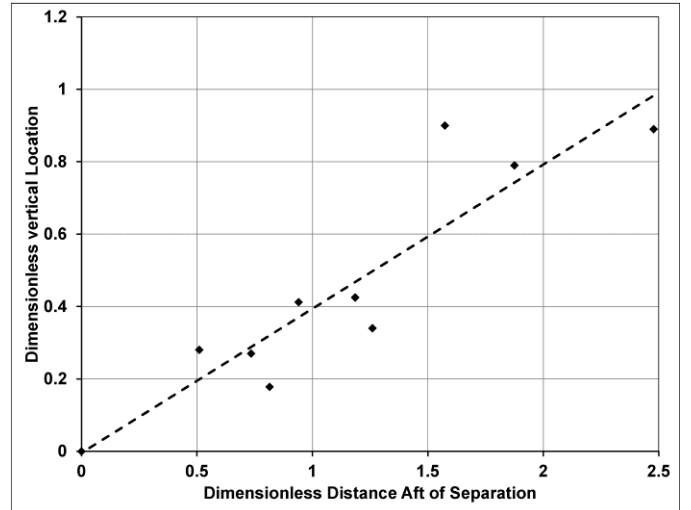


Figure 2 - Vertical Location of a Free Vortex

The wind tunnel data⁶ for the vertical location of a free vortex is shown in Fig. 2.

$$\text{Here, Dimensionless Vertical Location} = \frac{z_V - 1}{R}.$$

The data displayed above cover the angle of attack range from 10° to 30° , and extend aft from the body nose tip about 10 body diameters. The dashed line in Fig. 2 is a rough fit to the data that could be used in other analyses. Its equation is

$$\frac{z_V}{R} = 1 + 0.21 \frac{(x - x_s)\alpha}{R} \quad (3)$$

The image vortex is collinear with the centerline and the external vortex, but with opposite sign. It can be shown⁸ that if

$$rs = R^2 \quad (4)$$

the boundary condition on the cylinder surface is satisfied everywhere.

IV. ANALYSIS OF VORTEX-INDUCED ROLL MOMENT

First, consider the effects of vorticity shed from the fore body at high angles of attack. In the Reynolds no. range commonly encountered with sounding rockets at resonance a pair of vortices are shed into the leeward wake over the forebody. The vortex pair is initially symmetric about the angle of attack plane. As the leeward wake moves aft, the vortex pair grows stronger from additional vorticity shed from the body. In the neighborhood of the tail fins the vortex pair, and their image vortices induces a roll moment.

Figure 3 shows the important features of this problem. The solid dots represent the cores of the shed free vortices. The open dots represent the cores of the image vortices, located at a distance s from the centerline⁸. Each free-image vortex pair will satisfy the boundary condition of no flow through the cylindrical body surface. As described above the location and strength of the shed vortex pair (r, ϕ_v) must be found from wind tunnel experiment.

The fundamental assumption beneath the induced roll moment calculation is the idea of incompressible cross flow. That is, the flow in the cross flow plane may be considered incompressible so long as the overall hypersonic similarity parameter H is small compared to unity:

$$H = \sqrt{M^2 - 1} \sin(\alpha) \ll 1 \quad (5)$$

Since for roll lock-in the angle of attack is often less than about 0.2 radians, this implies the flight Mach number $M < 5$, or so. Equation (5) is automatically satisfied for subsonic free stream Mach numbers.

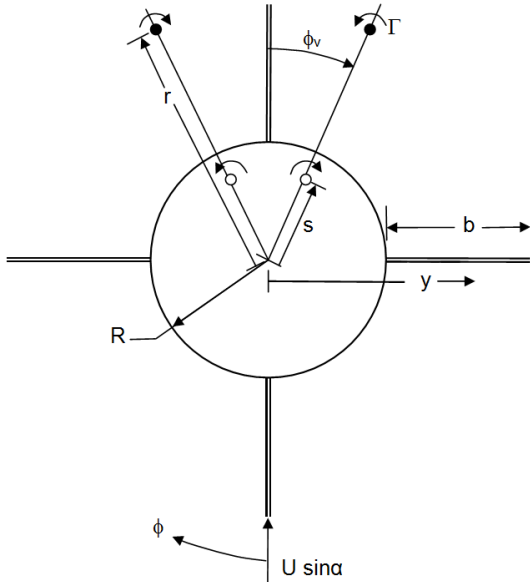


Figure 3 - Roll Geometry Looking Forward

The flow around an isolated vortex follows circular streamlines centered on the vortex⁸. The tangential velocity v_θ at a radial distance a from the vortex core to a point on a fin is

$$v_\theta = \frac{\Gamma}{2\pi a} \quad (6)$$

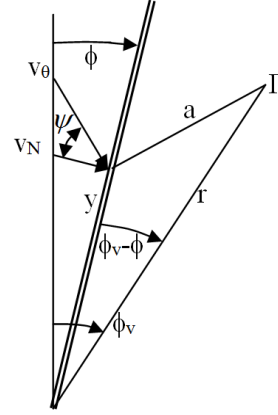


Figure 4 - Vortex and Fin in the Cross Flow Plane

The sign convention used here is to view the rocket from its nose tip. A positive Γ and v_θ follow the fingers of the right hand when the thumb points out of the paper. A positive roll moment also follows this right hand rule.

Now, look at Fig. 4, and consider the interaction between the fin at top dead center and the free vortex at ~ 2 o'clock. The distance between the vortex core and a point on the fin, a , is

$$a = \sqrt{y^2 + r^2 - 2yr \cos(\phi_v - \phi)} \quad (7)$$

Next, the angle ψ between the tangential velocity and the normal to the fin panel is

$$\psi = \pi - \cos^{-1}\left(\frac{a^2 + y^2 - r^2}{2ay}\right) \quad (8)$$

Then, the vortex-induced velocity normal to the fin panel is

$$v_N = v_\theta \cos \psi, \text{ or} \\ v_N = -\frac{\Gamma(y - r \cos(\phi_v - \phi))}{2\pi(y^2 + r^2 - 2yr \cos(\phi_v - \phi))} \quad (9)$$

Assuming a fin planform with straight taper, the local chord is given by

$$c(y) = C_1 + C_2 y, \text{ where} \quad (10)$$

$$C_1 = c_R \left(1 + \left(\frac{R}{b}\right)\right) - c_T \left(\frac{R}{b}\right) = c_R \left[1 + \left(\frac{R}{b}\right)(1 - \lambda)\right] = c_1 c_R \\ \text{and} \quad (11)$$

$$C_2 = -\frac{c_R - c_T}{b} = c_R \frac{\lambda - 1}{b} = c_2 c_R$$

With this the rolling moment due to a fin strip in the presence of an isolated vortex is

$$\begin{aligned} d(\text{Induced Moment}) &= -q\gamma c(y)dyC_{N\alpha} \frac{v_N}{U} \\ &= q\gamma(C_1 + C_2y)C_{N\alpha} \frac{\Gamma(y - r\cos(\phi_V - \phi))}{2\pi U(y^2 + r^2 - 2yr\cos(\phi_V - \phi))} dy \\ &= \frac{qC_{N\alpha}\Gamma}{2\pi U} \frac{(yC_1 + y^2C_2)(y - r\cos(\phi_V - \phi))}{(y^2 - 2yr\cos(\phi_V - \phi) + r^2)} dy, \text{ or} \end{aligned}$$

$$\begin{aligned} \text{Induced Moment (One Fin, One Vortex)} &= \\ &= \frac{qC_{N\alpha}\Gamma}{2\pi U} \int_R^{b+R} \frac{1}{y^2 - 2yr\cos(\phi_V - \phi) + r^2} \\ &\quad \left[-yC_1r\cos(\phi_V - \phi) \right. \\ &\quad \left. + y^2(C_1 - C_2r\cos(\phi_V - \phi)) + y^3C_2 \right] dy. \end{aligned} \quad (12)$$

To provide a useful result, this must be coded in a computer program. To this end define some functions:

$$\begin{aligned} f_0 &\equiv \int \frac{dy}{y^2 - 2yr\cos(\phi_V - \phi) + r^2} \\ &= \frac{1}{r\sin(\phi_V - \phi)} \tan^{-1} \left(\frac{y}{r\sin(\phi_V - \phi)} - \cot(\phi_V - \phi) \right) \end{aligned} \quad (13)$$

$$\begin{aligned} f_1 &\equiv \int \frac{ydy}{y^2 - 2yr\cos(\phi_V - \phi) + r^2} \\ &= \frac{1}{2} \log(y^2 - 2yr\cos(\phi_V - \phi) + r^2) + r\cos(\phi_V - \phi)f_0 \end{aligned} \quad (14)$$

$$\begin{aligned} f_2 &\equiv \int \frac{y^2 dy}{y^2 - 2yr\cos(\phi_V - \phi) + r^2} \\ &= y + r\cos(\phi_V - \phi) \log(y^2 - 2yr\cos(\phi_V - \phi) + r^2) \\ &\quad + r^2 \cos(2(\phi_V - \phi))f_0 \end{aligned} \quad (15)$$

and

$$\begin{aligned} f_3 &\equiv \int \frac{y^3 dy}{y^2 - 2yr\cos(\phi_V - \phi) + r^2} \\ &= \frac{y^2}{2} + 2yr\cos(\phi_V - \phi) + r^2(2\cos^2(\phi_V - \phi) - \frac{1}{2}) \\ &\quad \log(y^2 - 2yr\cos(\phi_V - \phi) + r^2) + r^3 \cos(3(\phi_V - \phi))f_0 \end{aligned} \quad (16)$$

We can now write the vortex-induced roll moment for one fin in the presence of one vortex in the form

$$= \frac{qC_{N\alpha}\Gamma}{2\pi U} g(C_1, C_2, r, \phi_V, y, \phi) \quad (17)$$

with the function g given by

$$\begin{aligned} g &= -C_1r\cos(\phi_V - \phi)f_1 \\ &\quad + (C_1 - C_2r\cos(\phi_V - \phi))f_2 + C_2f_3 \end{aligned} \quad (18)$$

The variable appears explicitly in eq. (17) because has not yet been evaluated at the limits of integration. The vortex-induced roll moment for a single fin is

$$= \frac{qC_{N\alpha}\Gamma}{2\pi U} \left(\begin{aligned} &\Delta g(\text{First quadrant free vortex}) \\ &- \Delta g(\text{First quadrant image vortex}) \\ &- \Delta g(\text{Second quadrant free vortex}) \\ &+ \Delta g(\text{Second quadrant image vortex}) \end{aligned} \right)$$

Here Δg is the definite integral form of the indefinite integrals given by eq. (18).

$$= \frac{qC_{N\alpha}\Gamma}{2\pi U} \left(\begin{aligned} &g(C_1, C_2, r, \phi_V, b+R, \phi) - g(C_1, C_2, r, \phi_V, R, \phi) \\ &- g(C_1, C_2, s, \phi_V, b+R, \phi) + g(C_1, C_2, s, \phi_V, R, \phi) \\ &- g(C_1, C_2, r, -\phi_V, b+R, \phi) + g(C_1, C_2, r, -\phi_V, R, \phi) \\ &+ g(C_1, C_2, s, -\phi_V, b+R, \phi) - g(C_1, C_2, s, -\phi_V, R, \phi) \end{aligned} \right) \quad (19)$$

The signs in the various terms of eq. (19) arise from integration limits and the signs of the various vortices.

The roll moment contribution from the second fin panel takes exactly the same form except that the roll angle argument ϕ is increased to $\phi + 2\pi/N$. The roll angle argument for each successive fin panel is increased by $2\pi/N$. The moment from each of N panels takes two function evaluations to implement the integration limits times four for the four vortices. For a four-finned configuration, 32 g function evaluations are needed for each roll angle.

Right-left symmetry is important. Assuming an airfoil normal force coefficient slope of 4 / radian, Fig. 6 below shows the induced roll moment coefficient for a four-finned rocket at various angles of attack as found by the methods of this paper. Note that for small angles of attack, the phasing can change by 180°. Figure 6 clearly shows the sinusoidal character of a typical induced moment curve. It follows that the induced moment can be represented well by a simple sine wave whose amplitude can be approximated by a single calculation at a roll angle of about $\pi/2N$. The maximum amplitude of C_{Li} over the entire roll angle range is shown as solid curve in Fig. 7.

V. LOCKED-IN LUNAR MOTION

Next, consider the steady state lunar coning motion of a rocket in roll lock-in. In lunar coning motion one side of the rocket always faces the spin rate vector $\bar{\omega}$ as shown in Fig. 5: A further description of this motion is: The rocket is assumed to be both slender and to have pitch-yaw symmetry. It follows that the roll moment of inertia can always be neglected when it appears in combination with the pitch or yaw moment of inertia.

The forcing function for this motion is assumed to be a combination of thrust misalignment and lateral C.G. offset acting in the pitch plane. Its palliation, mass balancing, is known to be easy and effective.

Because the motion is assumed to be steady state, the angle of attack α is assumed to be constant. In other words, the

rocket is in a "flat or lunar spin" with one side always facing inward.

Then the steady state roll (x-axis) and yaw (z-axis) rates are:

$$\begin{aligned} p &= \omega \cos \alpha \\ \text{and} \\ r &= -\omega \sin \alpha \end{aligned} \quad (20)$$

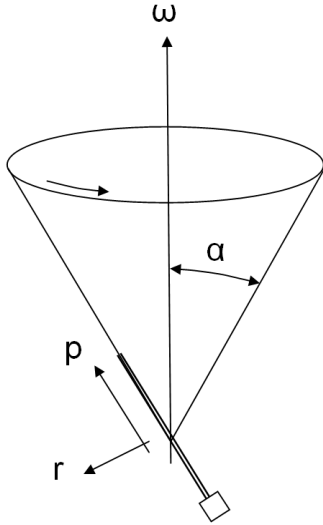


Figure 5 - Lunar Locked In Motion

In body-fixed axes the three equilibrium moment equations⁸ are

$$M_{Roll} = 2\pi q R^3 \left[C_{Lp} \frac{R\omega \cos \alpha}{U} + NC_{L\delta} \delta_F + C_{Li}(\phi, \alpha) \right] = 0 \quad (21)$$

and, assuming thrusting flight,

$$M_{Pitch} = 2\pi q R^3 C_{M\alpha} a + T(l_T \delta_T + \Omega) = I_p \omega^2 \sin \alpha \cos \alpha \quad (22)$$

The perturbations driving this motion, δ_T and Ω , are random. Some estimates on them can be found in refs. (15) and (16). The static pitching moment in eq. (22) above should be treated with respect. At sufficiently high angle of attack the fins are susceptible to stalling if the Mach number is subsonic.

Now, the derivative C_{Np} appearing in the third (M_{Yaw}) of these equations is tricky. If evaluated at zero α it will be found to vanish. But, if evaluated at a non-zero α it can have significant dynamic effects. It's basically a Magnus torque. That's because C_{Np} is really $C_{Np\alpha}$ as shown in the Appendix. Thus,

$$C_{Np} \frac{R\omega \cos \alpha}{U} = C_{Np\alpha} \frac{R\alpha \omega \cos \alpha}{U} \quad (23)$$

Then, the yaw moment equation becomes

$$\begin{aligned} M_{Yaw} &= 2\pi q R^3 \left[-C_{Nr} \frac{R\omega \sin \alpha}{U} + C_{Np\alpha} \frac{R\alpha \omega \cos \alpha}{U} \right] \\ &= -I_p \omega^2 \sin \alpha \cos \alpha \end{aligned} \quad (24)$$

These three equations have three unknowns, a , ω and ϕ . Combining the second and third gives:

$$\begin{aligned} 2\pi q R^3 C_{M\alpha} \alpha + T(l_T \delta_T + \Omega) \\ = 2\pi q R^3 \left[C_{Nr} \frac{R\omega \sin \alpha}{U} - C_{Np\alpha} \frac{R\alpha \omega \cos \alpha}{U} \right] \end{aligned}$$

Assuming the trim angle of attack is small lets us estimate α :

$$\alpha \cong \frac{-T(l_T \delta_T + \Omega)}{2\pi q R^3 \left[C_{M\alpha} + [C_{Np\alpha} - C_{Nr}] \frac{R\omega}{U} \right]}$$

Solve the third equation for ω under the same conditions:

$$\omega \cong \frac{2\pi q R^4}{U I_p} [C_{Nr} - C_{Np\alpha}] \quad (25)$$

Note as always the period P of the motion is $P = \frac{2\pi}{\omega}$.

Combining eq's. (24) and (25) results in:

$$\alpha \cong \frac{-T(l_T \delta_T + \Omega)}{2\pi q R^3 \left[C_{M\alpha} - \frac{2\pi q R^5}{U^2 I_p} (C_{Nr} - C_{Np\alpha})^2 \right]} \quad (26)$$

Equation (26) is important because it can be used to estimate the probability of not exceeding α . Due to roll symmetry, the pitch axis in this analysis is defined by the direction of the vector sum of the two transverse components of the perturbing torque. If the statistics of both transverse components have the same Gaussian distribution, then α has a Rayleigh distribution. Let

$$\text{var}(\alpha) = \frac{T^2 \text{var}(l_T \delta_T + \Omega)}{2\pi^2 q^2 R^6 \left[C_{M\alpha} - \frac{2\pi q R^5}{U^2 I_p} (C_{Nr} - C_{Np\alpha})^2 \right]^2}, \text{ where} \quad (27)$$

$$\text{var}(l_T \delta_T + \Omega) = l_T^2 \text{var}(\delta_T) + \text{var}(\Omega)$$

Then, the probability of exceeding α is

$$\text{Pr} = 1 - \exp \left[\frac{-\alpha^2}{\text{var}(\alpha)} \right] \quad (28)$$

Next, to find the maximum α for which no lock-in is possible, return to the roll equilibrium condition, eq. (21):

$$\left[C_{Lp} \frac{R\omega \cos \alpha}{U} + NC_{L\delta} \delta_F + C_{Li}(\phi, \alpha) \right] = 0$$

Now, at low angle of attack (just prior to entering the resonant condition),

$$NC_{L\delta}\delta_F = -C_{Lp} \frac{pR}{U}$$

The roll rate just before resonance is just the pitch natural frequency. Then

$$p = \omega_n = \sqrt{\frac{-2\pi q R^3 C_{M\alpha}}{I_p}}, \text{ and}$$

$$NC_{L\delta}\delta_F = -C_{Lp} \sqrt{\frac{-\pi \rho R^5 C_{M\alpha}}{I_p}}$$

With this, the roll equilibrium equation becomes

$$\frac{C_{Lp}}{U} \left[R\omega - \sqrt{\frac{-2\pi q R^5 C_{M\alpha}}{I_p}} \right] + C_{Li}(\phi, \alpha^*) = 0 \quad (29)$$

Equations (28) and (29) are the key to our problem. At small angles of attack, the C_{Li} term is too small to satisfy eq.(29) for any roll angle. That is, no steady state locked-in solution is possible. The smallest angle of attack α^* for which a steady state locked-in solution exists is given implicitly by

$$\left| \frac{C_{Lp}}{U} \left[R\omega - \sqrt{\frac{-2\pi q R^5 C_{M\alpha}}{I_p}} \right] \right| \leq |C_{LiMAX}(\alpha^*)| \quad (30)$$

where $C_{LiMAX}(\alpha^*)$ is the maximum value of C_{Li} obtained by finding ϕ , at a fixed angle of attack, that roll angle ϕ which maximizes/minimizes C_{Li} . Since the induced roll moment oscillates between positive and negative maximum values, equation (30) should be interpreted to mean, for a lock-in solution to exist, that the C_{Li} term has a sign opposite to that of the C_{Lp} term. In effect, eq. (30) defines a necessary and sufficient condition for roll lock-in to occur. Unless it is satisfied, roll lock-in cannot happen, even though the perturbing torque is very large. But, if it is satisfied, then it's only a matter of statistics as shown in eq. (28).

VI. EXAMPLE

As an example of this process, consider the following set of parameters:

$U = 10000 \text{ in/sec}$	$q = 4 \text{ lb/in}^2$	$L = 122 \text{ in}$
$W = 60 \text{ lb}$	$X_{CG} = 71 \text{ in}$	$I_p = 27734 \text{ sl-in}^2$
$b = 6 \text{ in}$	$Rad = 3 \text{ in}$	$\beta = 2$
$\lambda = 0.3$	$SM = 3.33 \text{ cal}$	$SM = 20 \text{ in}$
$C_{N\alpha n} = 2 / \text{rad}$	$C_{N\alpha a} = 4 / \text{rad}$	$X_S = 36 \text{ in}$
$X_{CPF} = 108 \text{ in}$	$X_{CPN} = 39 \text{ in}$	$N = 4$

First, estimate the vortex-induced roll moment as a function of roll angle and plot it in Fig. 6 below:

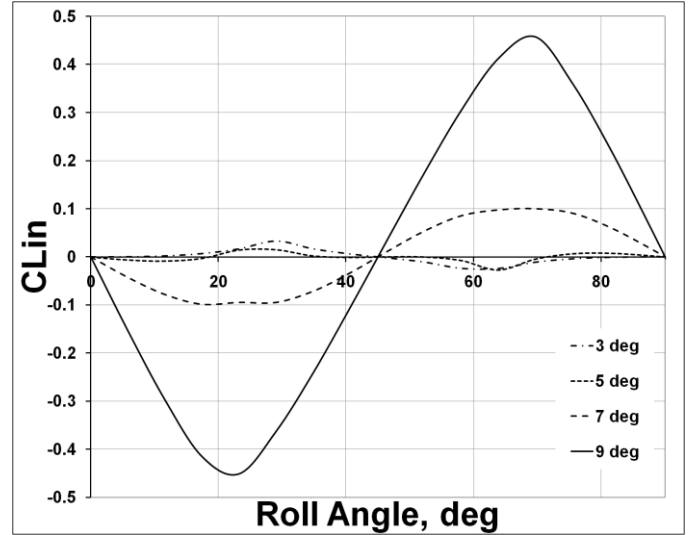


Figure 6 - Vortex-Induced Roll Moment for Various Angles of Attack

Figure 6 shows the induced roll moment vs. roll angle at angles of attack = 0.05, 0.1, 0.12 and 0.15 radians for the example vehicle. First, note that the roll moment vs. roll angle curve goes through a 180° phase change from a small angle attack regime ($\alpha < 6^\circ$) to different regime at larger angles of attack. As α increases beyond this transition, the amplitude of the induced roll moment increases to very large values. This is caused by the changing position of the fin tips relative to the shed vortex pair. This pattern is generally observed for many different fin geometries and flight conditions.

Next, consider how this leads to roll lock-in. Begin by finding the maximum value of C_{Li} as a function of angle of attack. This is shown as the solid line hill-valley-mountain curve in Fig. 7 below. When the number of fins is increased to, say 6, the single humped shape (think dromedary) shown in Fig. 7 often changes to a two humped (think Bactrian camel) form. If lock-in were to occur it would first manifest itself at these relative maximum α 's because at other roll angles (same α) the necessary induced roll moment would not be as large. The horizontal line in Fig. 7 corresponds to possible roll lock-in conditions. In regions with a thin, solid horizontal line roll lock-in cannot occur (not enough C_{Li}), but where the heavy dashed line appears, steady state roll lock-in can happen.

During the run up to pitch-roll resonance the angle of attack starts small and increases as resonance is approached. Lock-in will then be observed where the vertical dot-dashed line labeled α intersects the other two curves.

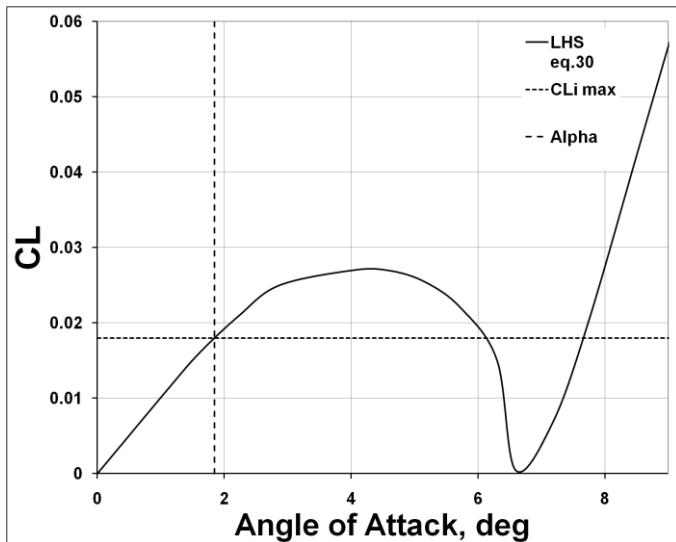


Figure 7 – Typical Conditions for Roll Lock-in

Figure 7 above sketches the approach to solving eq. (30) with the horizontal line representing the C_{Lp} term. To this varying amounts of C_{Li} are added with more as the angle of attack is increased. Lock-in first becomes possible when the maximum C_{Li} is just tangent to the horizontal line. Thus, eq.(30) implicitly defines the minimum angle of attack for lock-in. Now, since the first (C_{Lp}) term in eq. (30) does not depend on roll angle, the boundary between no roll lock-in and just possible roll lock-in is that C_{Li} be stationary with respect to roll angle, and that it be large enough to just balance the C_{Lp} term. Thus, at any specified angle of attack, there is a maximum / minimum for C_{Li} . This can be found using numerical methods from the induced roll moment data like that plotted in Fig. 6 above.

Now add in the remainder of eq. (30) as depicted in Fig. 7. The left hand side, the C_{Lp} term, appears as a horizontal straight line. Those parts of this straight line shown as heavy dashed lines are regions where roll lock-in is possible, that is, where eq. (30) is satisfied. Equation (26) establishes a pitch perturbing torque needed for the lowest angle of attack for roll lock-in shown by the vertical line in Fig. 7. Thus, no roll lock-in is possible in the region to the left of this vertical line. Given this, eq. (28) can be used to estimate the probability that no roll lock-in can occur.

VII. IMPLICATIONS FOR FIN DESIGN

Begin by observing that there is no guaranteed fin design that will always prevent roll lock-in. It is always possible to have very large misalignment torques that, no matter how statistically rare, will cause roll lock-in. But, it is possible to design fins that have a very low probability of lock-in. Figure 7 shows that if we can move the horizontal line high enough to clear the “hill” lock-in will be deferred to very high, and uncommon, angles of attack.

Once we have a model of vortex-induced roll moment and how it influences roll lock-in, it is appropriate to consider what can be done to mitigate steady state roll lock-in. The obvious first thing is to carefully roll-balance and align the structure to minimize the pitch / yaw perturbing torques. This has been known for a very long time.

So the next step in our mitigation strategy is to try to hold the left hand side of eq. (30) above the C_{Li} hump(s) occurring low angle of attack. In achieving this goal, static margin is more important than generally realized. There is a long tradition of designing for two calibers (body diameters) of static margin. But Fig. 8 shows that, apart from the perturbing torque statistics, more than two calibers can extend the region where lock-in is dynamically impossible.

The left hand side of eq. (30) depends significantly on flight condition, more specifically dynamic pressure as shown in Fig. 9 below. Larger dynamic pressure acts like larger static margin by reducing angle of attack. It is expected that the smaller dynamic pressures at higher altitude will exacerbate any lock-in tendencies.

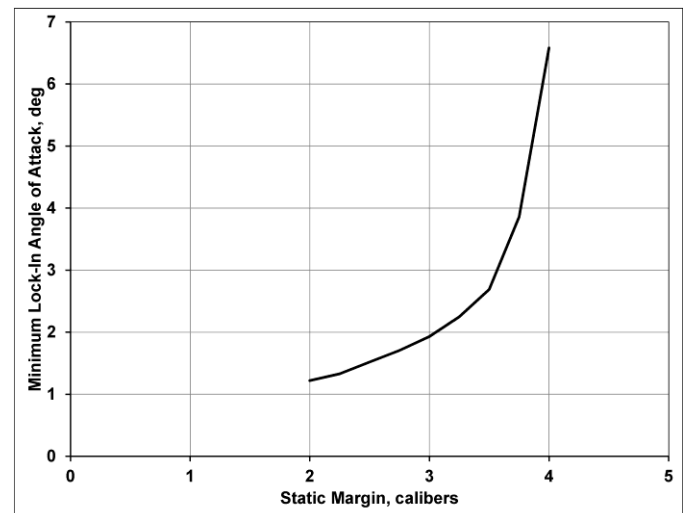


Figure 8 - Typical Effects of Varying Static Margin

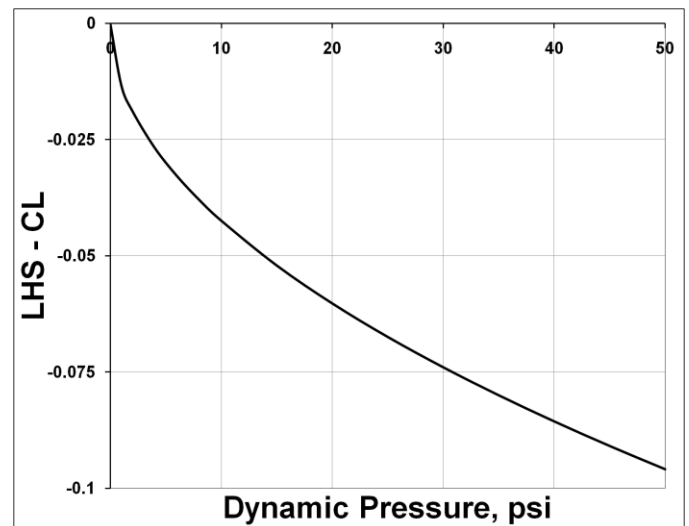


Figure 9 - Effect of Dynamic Pressure on the First (C_{lp}) Term in Eq. 30)

The remaining choices involve manipulating fin geometry. Fin design usually is one of the last steps in vehicle design. The Fin Designer considers most of the key system parameters identified in the example as givens. His free variables are fin size (Static Margin), number of fin panels (N) and fin shape (β and λ). The simplest approach is to manipulate the appearance of Fig. 7 by varying SM , N , β and λ to move the horizontal line above the camel's hump(s).

By far the most important fin parameter for mitigating lock-in is the number of fin panels, N . Most sounding rockets have flown with 4 fins with a small minority using only 3 fins, and almost none with 5 or more. Our model shows that there is very little difference between 3 and 4 fins when attempting implementation of the first part of our strategy. Small tweaks in taper ratio λ or exposed fin span β can bring about very similar performance in these two cases. But, increasing the number of fins to 5 or more leads to dramatic improvements. Our model shows that with 6 fins major improvement is relatively easy, and it becomes trivially easy with 8. Note that mortar bombs are commonly flown with 8 fin panels.

Assuming the same baseline for all fin counts, results are shown in Fig's. 10, 11, 12 and 13 for 3, 4, 6 and 8 fin panels.

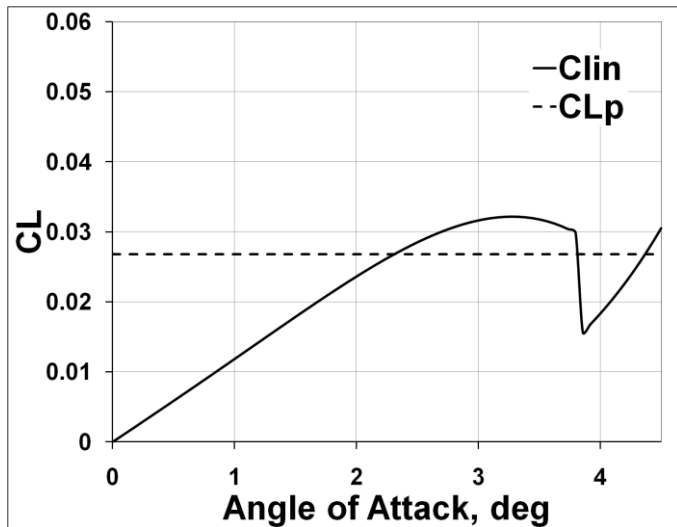


Figure 10 - CL of 3 fins for Various Angles of Attack

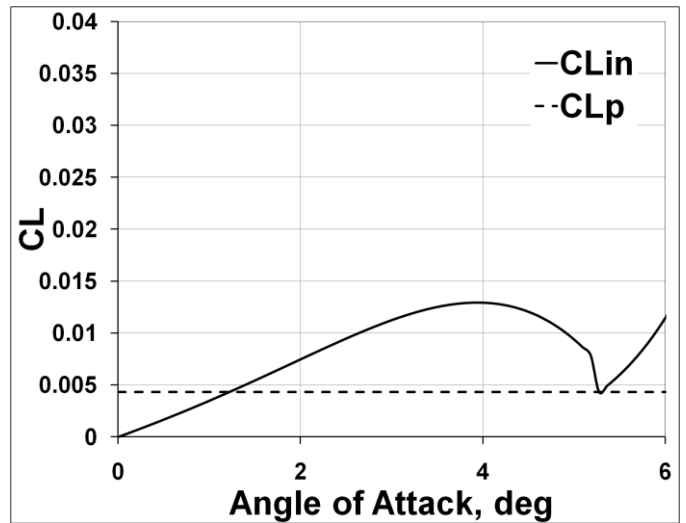


Figure 11 - CL of 4 fins for Various Angles of Attack

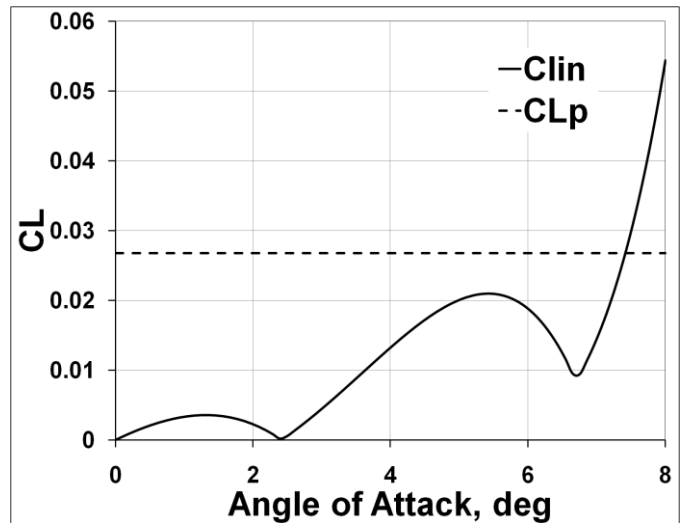


Figure 12 - CL of 6 fins for Various Angles of Attack

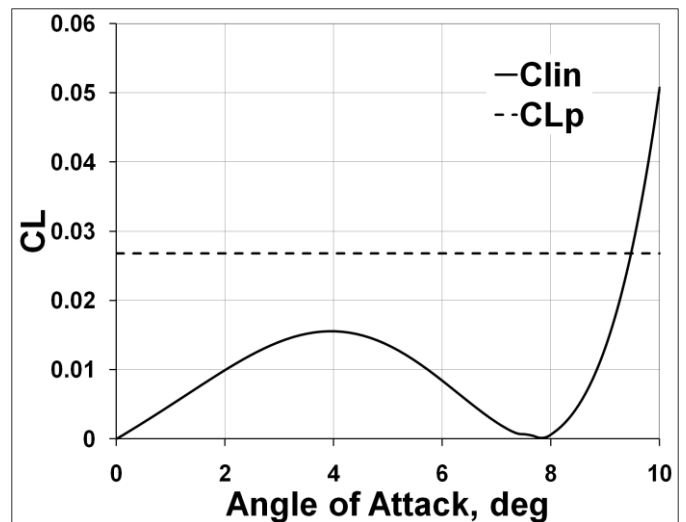


Figure 13 - CL of 8 fins for Various Angles of Attack

The effect of increasing the number of fins beyond 4 dramatically, improves resistance to roll lock-in.

VIII. RECOMMENDATION

To improve resistance to roll lock-in, consider using static margins greater than two calibers and more than four fins.

REFERENCES

- [1] Nicolaides, J. D., "A History of Ordnance Flight Dynamics", A.I.A.A. paper 70-533, 1970.
- [2] Platus, D. H., "Ballistic Re-entry Vehicle Flight Dynamics", J. Guidance, Vol. 5, no. 1, pp 4-16 (1982).
- [3] Ananthkrishnan, N., and Raisinghani, S. C., "Steady and Quasisteady Resonant Lock-in of Finned Projectiles", Journal of Spacecraft and Rockets, Vol. 29, no. 5, 1992, pp 692-696.
- [4] Clare, T.A., "Resonance Instability for Finned Configurations Having Nonlinear Aerodynamic Properties", Journal of Spacecraft and Rockets, Vol. 8, No. 3, 1971, pp 278-283.
- [5] Jorgensen, L. H. and Perkins, E. W., "Investigation of Some Wake Vortex Characteristics of an Ogive-Cylinder at Mach Number 2", N.A.C.A. Report 1371, 1955.
- [6] Thomson, K.D. and Morrison, D. F., "The Spacing, Position and Strength of Vortices in the Wake of Slender Cylindrical Bodies at Large Incidence", Journal of Fluid Mechanics, Vol. 50, Issue 04, 1971.
- [7] Spahr, J. R., "Theoretical Prediction of the Effects of Vortex Flows on the Loading, Forces, and Moments of Slender Aircraft", N.A.S.A. Technical Report R-101, 1961.
- [8] Rauscher, M., "Introduction to Aeronautical Dynamics", John Wiley & Sons, New York, 1953.
- [9] Hout, C. P., "Strip Theory for Setting Fin Angles (revised)", RST Memo, 13 September 2009.
- [10] Barrowman, J.S. and Barrowman, J.A., "The Theoretical Prediction of the Center of Pressure", Master of Science thesis, Catholic University, 1966.
- [11] Babister, A. W., "Aircraft Dynamic Stability and Response", Pergamon Press, London, 1980.
- [12] Naselius, K. A., "A Wind Tunnel Study of Magnus Effects on a Differentially Rotating Missile", AFIT M. S. Thesis, 1992.
- [13] Reid, E. G., "Tests of a Rotating Cylinder", N.A.C.A. TN-209. 1924.
- [14] Jacobson, I. D., "Magnus Characteristics of Arbitrary Rotating Bodies", AGARD-AG-171, edited by P. F. Yaggy, Harford House, London, England, 1973.
- [15] R. L. Ammons and C. P. Hout, "Standardized Perturbation Values for Several Sounding Rockets to be Used in the Calculation of Dispersion and Structural Loads", Aerojet-General Corporation memo 8110:M0658:ak, 16 September 1970.
- [16] R. N. Knauber, "Thrust Misalignments of Fixed-Nozzle Solid Rocket Motors", Journal of Spacecraft and Rockets, November-December 1996, pp794-799.
- [17] Abbott, I. H., von Doenhoff, A. E., and Stivers, L., Jr., "Summary of Airfoil Data", N.A.C.A. Report 824, 1945.

APPENDIX I: STABILITY DERIVATIVES

Strip theory⁹ considers a fin panel to have only two dimensions; that is, it's a pure airfoil. However, use of a 2D airfoil lift curve slope can give highly erroneous results so the reader is advised to use the 3D lift curve slope averaged over the exposed fin area. Now, consider Fig. 14 below. The local angle of attack α_{local} on an airfoil strip is

$$\alpha_{local} = \alpha(1 + (R/y)^2) + \delta - \omega_R y / U + \sum_1^N \alpha_{in} \quad (31)$$

where the second term in α is the inverse square upwash around a cylinder⁸. The third term is the fin cant angle, the fourth is due to roll damping and the last is the sum of the α_{in} 's induced by the four vortices.

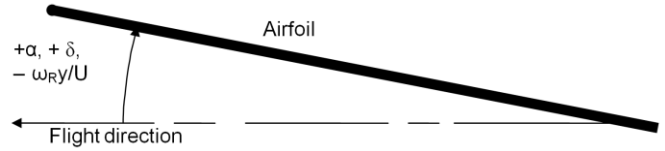


Figure 14 - Airfoil Sketch

Before analyzing the roll moments, take a break and recall that while we are trying to design fins to minimize nonlinear roll behavior, any resulting design must have the necessary static margin. This implies that the constraint takes the form of eq. (33) below¹⁰,

$$d(\text{Fin Normal Force Slope}) = q C_{N\alpha} c(y) dy \left(1 + \frac{R^2}{y^2}\right) \quad (32)$$

The last term accounts for body-fin upwash interference⁸. Integrating across the exposed fin span gives the single panel result,

Single Panel Fin Normal Force Slope =

$$q C_{N\alpha} c_R \left(\begin{array}{l} c_1 b + c_2 (b^2 + 2bR) / 2 + c_1 R^2 b / (R(b+R)) \\ + c_2 R^2 \log((b+R)/R) \end{array} \right)$$

For a complete symmetric fin configuration ($N \geq 3$) it can be shown¹⁰ that the

Total Fin Assembly Normal Force Coefficient Slope =

$$C_{N\alpha F} = C_{N\alpha} \frac{N c_R}{2\pi R^2} \left(\begin{array}{l} c_1 b + c_2 (b^2 + 2bR) / 2 \\ + c_1 R^2 b / (R(b+R)) \\ + c_2 R^2 \log((b+R)/R) \end{array} \right) \quad (33)$$

Keep in mind that the tail fins are the most important contributor to vehicle static margin. The static margin, and hence the fin assembly normal force slope, result from requirements unconnected to roll lock-in. Therefore eq's. (33) and (37) acts as a constraint on the allowable changes in fin geometry. To apply it, select $C_{N\alpha}$, b , R and λ . Solve for c_R .

Then, the roll driving and damping moments of a single fin panel⁹ are

$$\begin{aligned} \text{Driving Moment} &= q C_{N\alpha} \delta \int_R^{b+R} y c(y) dy \\ &= q C_{N\alpha} \delta \left[\left(\frac{C_1}{2}\right) y^2 + \left(\frac{C_2}{3}\right) y^3 \right] \\ &= q C_{N\alpha} \delta \left[\begin{array}{l} \left(\frac{C_1}{2}\right) (b^2 + 2Rb) \\ + \left(\frac{C_2}{3}\right) (b^3 + 3Rb^2 + 3R^2b) \end{array} \right] \end{aligned}$$

$$C_{L\delta} = \frac{C_{Na}c_R}{2\pi R^3} \left[\begin{aligned} & \left(\frac{c_1}{2}\right)((b+R)^2 - R^2) \\ & + \left(\frac{c_2}{3}\right)((b+R)^3 - R^3) \end{aligned} \right] \quad (34)$$

$$\begin{aligned} \text{Damping Moment} &= -qC_{Na} \frac{p}{U} \int_R^{b+R} y^2 c(y) dy \\ &= -qC_{Na} \frac{p}{U} \left[\begin{aligned} & \left(\frac{C_1}{3}\right)(b^3 + 3Rb^2 + 3R^2b) \\ & + \left(\frac{C_2}{4}\right)(b^4 + 4b^3R + 6R^2b^2 + 4R^3b) \end{aligned} \right] \\ C_{Lp} &= -\frac{C_{Na}c_R}{\pi R^4} \left[\begin{aligned} & \left(\frac{c_1}{3}\right)((b+R)^3 - R^3) \\ & + \left(\frac{c_2}{4}\right)((b+R)^4 - R^4) \end{aligned} \right] \end{aligned} \quad (35)$$

The stability derivatives needed for the lunar coning version of roll lock-in are estimated above.

A. $C_{M\alpha}$

A simple estimate on the static margin is

$$SM = x_{CP} - x_{CG} = \frac{x_{CPN}C_{NaN} + x_{CPF}C_{NaF}}{C_{NaN} + C_{NaF}} - x_{CG}$$

the static pitching moment derivative is then

$$dC_{M\alpha} = x_{CG}(C_{NaN} + C_{NaF}) - x_{CPN}C_{NaN} - x_{CPF}C_{NaF} \quad (36)$$

Finally, the required fin assembly normal force coefficient slope is

$$C_{NaF} = C_{NaN} \frac{-SM + x_{CPN} - x_{CG}}{SM - x_{CPF} + x_{CG}} \quad (37)$$

This is used in eq. (33).

B. C_{Nr}

The yaw moment due to roll rate can be estimated for a single fin panel using the strip theory methods of ref. (10). First, the definition of the yaw moment coefficient:

$$C_N = \frac{N}{qSR}$$

Its derivative with respect to $pR/2U$ is defined as C_{Np} .

Now, decompose the body into a sequence of elements, each of which has a normal force coefficient slope c_{Na} . If an element were located a distance $\Delta x_i = x_{CG} - x_i$ from the center of mass, then

$$C_{Nr} = -2 \sum c_{Na_i} \left(\frac{\Delta x_i}{R}\right)^2 \quad (38)$$

where the summation extends over all body elements including those with fins.

C. $C_{Np\alpha}$

The yaw moment due to rolling and angle of attack is tricky because it requires estimation of the Magnus force on the body. Reference (13) provides an experimental estimate of the Magnus side force acting on a uniform spinning cylinder:

$$C_Y = 0 \text{ when } \frac{Rp}{U \sin \alpha} \leq 0.5 \quad (39)$$

Since this condition is abundantly satisfied for the current problem ($\frac{Rp}{U \sin \alpha} \approx 0.05$), the body contribution to Magnus moment can be neglected. But, the data^{8,12,13,14} show that there is a significant nonlinearity near zero roll rate. Once the condition in eq. (39) is exceeded, the side force increases more or less linearly with $\frac{Rp}{U \sin \alpha}$.

The fin contribution can be found with the aid of Fig. 15 below. Consider a strip of fin of span dy viewed from the left. While the basic, non-rolling angle of attack is still $\alpha \cos \phi$ there is a additional local angle of attack due to roll rate:

$$\alpha_p = \frac{py}{U \cos \alpha}$$

If we define lift L and drag D the usual way, normal to and parallel the relative velocity vector, the x -force X acting on the chordwise strip for small α is:

$$dX = (\alpha \cos \phi + \frac{py}{U})dL - dD$$

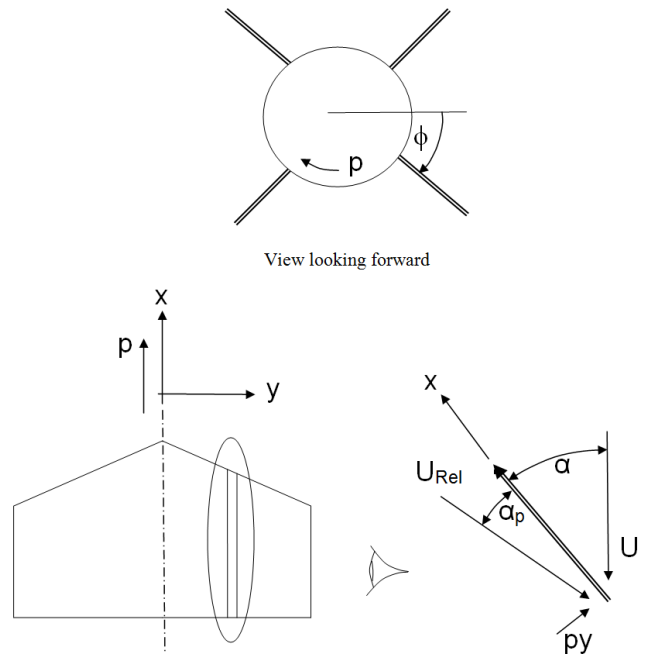


Figure 15 - Rolling Fin Geometry

The yawing moment contributed by the strip is

$$dN = -y \cos \phi (\alpha_{local} \cos \phi + \alpha_p) dL - dD$$

Next, recall that body upwash adds to the local lift distribution, and that $C_{L\alpha} \approx C_{N\alpha}$. Then,

$$dN = -q \cos \phi \left(\begin{array}{l} (\alpha(1 + \frac{R^2}{y^2}) \cos \phi + \frac{py}{U}) \\ C_{N\alpha} (\alpha(1 + \frac{R^2}{y^2}) \cos \phi + \frac{py}{U}) - C_D \end{array} \right) ycdy$$

Converting to coefficient form, and noting that a symmetrical airfoil drag has a parabolic relationship with local angle of attack,

$$C_D = C_{D0} + \frac{1}{2} \frac{\partial^2 C_D}{\partial \alpha^2} \alpha_{local}^2 \sin^2 \Lambda$$

$$dC_N = -\frac{\cos \phi}{2\pi R^3} (C_{N\alpha} - \frac{\partial^2 C_D}{\partial \alpha^2} \sin^2 \Lambda) (\alpha(1 + \frac{R^2}{y^2}) \cos \phi + \frac{py}{U})^2 ycdy$$

Retaining only those terms contributing to $C_{Np\alpha}$, results in

$$dC_N = -\left(\frac{(C_{N\alpha} - C_{D\alpha\alpha} \sin^2 \Lambda) \cos^2 \phi}{\pi R^3} \right) \alpha \frac{p}{U} (1 + \frac{R^2}{y^2}) (C_1 y^2 + C_2 y^3) dy \quad (40)$$

The single panel stability derivative is found after integrating from R to $b+R$, and differentiating:

$$C_{Np\alpha} = -\left(\frac{(C_{N\alpha} - C_{D\alpha\alpha} \sin^2 \Lambda) \cos^2 \phi}{\pi R^4} \right) \left(\begin{array}{l} \frac{C_1}{3} ((b+R)^3 - R^3) + \frac{C_2}{4} ((b+R)^4 - R^4) \\ + R^2 (C_1 b + \frac{C_2}{2} ((b+R)^2 - R^2)) \end{array} \right)$$

The full fin assembly $C_{Np\alpha}$ requires adding the terms from all fin panels. Thus, for $N \geq 3$,

$$C_{Np\alpha} = -\left(\frac{N C_R (C_{N\alpha} - C_{D\alpha\alpha} \sin^2 \Lambda)}{2\pi R^4} \right) \left(\begin{array}{l} \frac{C_1}{3} ((b+R)^3 - R^3) + \frac{C_2}{4} ((b+R)^4 - R^4) \\ + R^2 (c_1 b + \frac{C_2}{2} ((b+R)^2 - R^2)) \end{array} \right) \quad (41)$$

Two comments are in order. Due to root and tip effects, $C_{N\alpha}$ will vary across the fin span. A good first approximation is to take the full, 3D $C_{N\alpha}$ without body upwash, and average it over the span. Second, the derivative $C_{D\alpha\alpha}$ can be estimated from wind tunnel measurements¹⁷. Typically, $C_{D\alpha\alpha} \cong 0.2$, or

so, in incompressible flow. For fins with supersonic leading edges, the Ackeret result for airfoil wave drag should be used. The correction for sweep angle is based on infinite swept wing theory.

APPENDIX II: CENTER OF MASS OFFSET MOMENT

A second major source of nonlinear roll moment of offset center of mass. This is sketched in Fig. 16 below

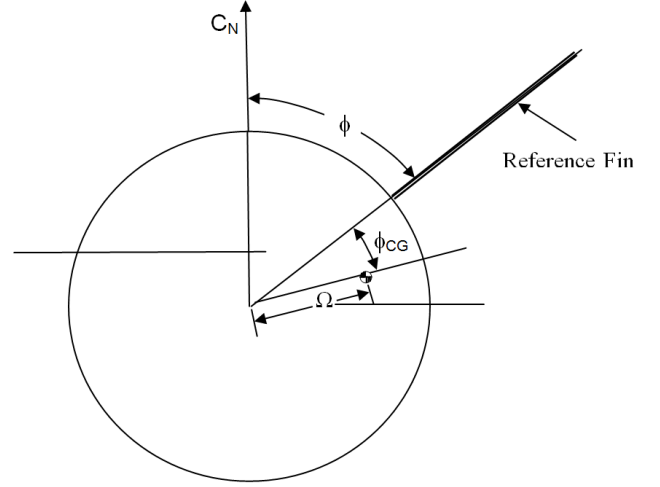


Figure 16 - Roll moment due to Center of Mass Offset

We easily find that the induced roll moment is

$$C_{LCG} = \frac{\Omega}{d} C_{N\alpha} \alpha \sin(\phi + \phi_{CG}) \quad (42)$$

The total nonlinear roll moment is then the sum of that due to nose vorticity and that due to CG offset, including statistical correlations